RSC Advances

This is an *Accepted Manuscript*, which has been through the Royal Society of Chemistry peer review process and has been accepted for publication.

Accepted Manuscripts are published online shortly after acceptance, before technical editing, formatting and proof reading. Using this free service, authors can make their results available to the community, in citable form, before we publish the edited article. This *Accepted Manuscript* will be replaced by the edited, formatted and paginated article as soon as this is available.

You can find more information about *Accepted Manuscripts* in the Information for Authors.

Please note that technical editing may introduce minor changes to the text and/or graphics, which may alter content. The journal's standard Terms & Conditions and the Ethical guidelines still apply. In no event shall the Royal Society of Chemistry be held responsible for any errors or omissions in this *Accepted Manuscript* or any consequences arising from the use of any information it contains.

ROYAL SOCIETY OF CHEMISTRY

www.rsc.org/advances

Journal Name

RSCPublishing

ARTICLE

Hierarchical flower-like Bi_2WO_6 hollow microspheres: facile synthesis and excellent catalytic performance

Cite this: DOI: 10.1039/x0xx00000x

Peigen Zhang[a, b], Jian Zhang[a], Anjian Xie[a, b], Shikuo Li[a, b], Jiming Song[a], Yuhua Shen[a, b,*]

Received 00th January 2012,
Accepted 00th January 2012

DOI: 10.1039/x0xx00000x

www.rsc.org/

One step method has been developed for the fabrication of hierarchical flower-like Bismuth tungstate (Bi_2WO_6) hollow spheres via a solvothermal process. The size of these microspheres is about 1.5 μm, and the shells are composed of nanosheets with a thickness of about 15 nm. Specifically, the product has a specific surface area of 95 m^2 g^{-1}. The formation mechanism of flower-like Bi_2WO_6 is proposed, which involves the nucleation and formation of nanoparticles followed by their self-assembly to microspheres, oriented growth, Ostwald ripening and transformation into flower-like hollow microspheres. The Bi_2WO_6 hollow spheres exhibit excellent visible light catalytic efficiency for the degradation of Rhodamine B (RhB), up to 98% within 50 min. The efficiency retains 92% after five photodegradation cycles due to the hierarchical hollow structure and large surface area.

Introduction

Recently, the photocatalysts have caused a considerable concern because they play a very important role in solving environmental and pollution problems, employing solar energy for the catalytic degradation of organic pollutants. Therefore, friendly and highly efficient photocatalyst has aroused great interest. And these photocatalysts should have the following three characteristics including absorbing sunlight with an appropriate energy band, a longer lifetime of electron hole and conduction (valence) band with a more negative (positive) electrode potential. The researchers have developed a series of narrow band semiconductor photocatalytic materials, such as WO_3, Fe_2O_3 and CdS etc.[1], to make more effective use of solar energy. For the purpose of treating environmental organic pollutants, the synthesis of visible light catalysts has become a hotspot and gets more and more meaningful via a more effective and convenience approach.

Bi_2WO_6 is a layered Aurivillius oxide [2] with a narrow width of band gap. It can be excited by the visible light, improving the utilization of solar energy. As research shows that Bi_2WO_6, owing to its appropriate valence band and thermodynamic property, can decompose water and can be employed in the degradation of chloroform, acetaldehyde and other harmful substances under visible light[3], indicating the high photocatalytic efficiency of Bi_2WO_6. As we know, the morphology and structure of the photocatalysts have direct effect on their photocatalytic activity. For the past years, there were some reports that the Bi_2WO_6 photocatalysts with different morphologies are synthesized by different methods. For instance, Li et al. [4] obtained layered Bi_2WO_6 microspheres by utilizing PVP as the template; Amano et al.[5] synthesized the spark Bi_2WO_6 microspheres in aqueous solution with low pH values; Chen et al. [6] prepared Bi_2WO_6 microspheres by an inorganic salts-assisted hydrothermal method; Shang et al.[7] fabricated Bi_2WO_6 nanocages with unique morphologies by using carbon spheres as a template. Compared with the hard template method, the soft template method has some advantages, such as inexpensive, simple processing and easy to recycle, which makes the cost decreased in industrial applications. So it is important to synthesize Bi_2WO_6 photocatalyst by choosing proper soft template.

As we all know, ethylene glycol, a non-aqueous solvent with –OH group, has a good water or alcohol solubility, which is easy to be treated. It is widely used in the synthesis of monodisperse metal and metal oxide nanoparticles, and also as a soft template of the highly ordered structural material [8]. Ethanol forms the hydrogen bonding network easily due to the presence of the hydroxyl group. Therefore, we use a mixture of ethylene glycol and ethanol as both solvent and template to synthesize highly ordered flower-like porous and hollow Bi_2WO_6 microspheres by solvothermal method. The as-prepared product possesses high stability and excellent photocatalytic activity for the photodegradation of RhB. The formation and growth mechanism of hierarchical flower-like Bi_2WO_6 is worth exploring, originated in the observation of intermediate products obtained at different reaction stages. The

RSC Advances Accepted Manuscript

hollow Bi_2WO_6 catalyst will have potential application in water treatment.

Experimental

Materials

Bismuth nitrate pentahydrate ($Bi(NO_3)_3·5H_2O$), sodium tungstate dihydrate ($Na_2WO_4·2H_2O$), rhodamine B and ethanol were supplied by Shanghai Chemical Reagent Co. Ltd (P. R. China). Ethylene glycol (EG) was obtained from Sinopharm Chemical Reagent Co. Ltd (P. R. China).

All reagents were of analytical grade and used without further purification. Milli-Q water (Millipore Corp., with resistivity of 18.2 MΩ cm) was employed for all experiments.

Synthesis of flower-like hollow Bi_2WO_6 microspheres

Flower-like Bi_2WO_6 microspheres were synthesized via a solvothermal method. Bi $(NO_3)_3·5H_2O$ (2.5 mmol) and $Na_2WO_4·2H_2O$ (1.25 mmol) were dissolved in 12.5 mL of ethylene glycol, respectively. Then, $Na_2WO_4·2H_2O$ solution was added dropwise into Bi $(NO_3)_3·5H_2O$ solution with magnetic stirring, which was followed by the addition of absolute ethanol (25 mL). After stirring for 30 minutes, the mixed solution was transfered into a 100 mL Teflon lined autoclave at 160 °C for 12 h, respectively. The Teflon lined autoclave naturally cooled down to room temperature. The products were isolated by centrifugation and washed several times by doubly distilled water and absolute ethanol. Finally, the products were dried at 60 °C for 24 h in vacuum oven and reserved. Some experiments were carried out to control the morphologies of the samples, in which several reaction parameters such as reaction time, or the volume ratio of EG to ethanol (V_{EG}:V_E) were altered while other reaction conditions were kept constant.

Characterization

Transmission electron microscopy (TEM) measurements were carried out on JEM model 100SX electron microscopes (Japan Electron Co.) operated at an accelerating voltage of 80 kV. Field emission scanning electron microscopy (FESEM) measurements were taken with a Hitachi S4800 scanning electron microscope. The phase structure and phase purity of the as synthesized products were examined by X-ray diffraction (XRD), using a MAP18XAHF instrument, with the X-ray diffractometer using Cu-Ka radiation (λ= 1.5406 Å) at a scan rate of 6º/min. The accelerating voltage and applied current were 30 kV and 25 mA, respectively (MAC Science, Japan). Energy-dispersive spectra (EDS) were examined on a JEM-2010F high-resolution transmission electron microscope equipped with EDS detector working at an accelerating voltage of 200 kV. UV-vis diffuse reflectance spectra of the samples were obtained using a UV-vis solid spectrometer (Shimadzu SolidSpec-4100) by using $BaSO_4$ as a reference. Room temperature PL spectra were recorded on an F-4500 at room temperature (Japan Electron Co.). The specific surface area was estimated using the Brunauer–Emmett–Teller (BET) equation based on the nitrogen adsorption isotherm obtained with a Micromeritics ASAP 2020 Analyzer (Surface Area and Porosity System).

Photocatalytic activity of the products

The decolorization of a model pollutant RhB dye was chosen to evaluate the photocatalytic activity of the flower-like hollow Bi_2WO_6 microspheres under visible light. The 50 mg of Bi_2WO_6 is dispersed in 50 mL of RhB solution (1.0×10^{-5} mol L^{-1}). The solution was stirred for 30 min to ensure the catalyst was completely dispersed and a balance of adsorption and desorption of the catalyst in dark condition. The photocatalytic experiment was carried out in a self-designed reactor, using a 500 W xenon lamp equipped with a 420 nm cut-off filter to provide visible light irradiation, which was placed 6 cm above the reaction slurry. The concentration changes of the RhB in photodegradation process were measured by UV-vis spectrophotometer. In the each recycling experiment, the flower-like hollow Bi_2WO_6 microspheres were separated from solution after photocatalytic degradation of RhB, then washed with ethanol and deionized water three times respectively before being redispersed in the same concentration and volume of RhB solution for another cycle. Some control experiments were carried out to study the degradation of RhB. Several reaction parameters, for instance, pH values or concentrations of the RhB solutions were varied while other reaction conditions remained constant.

Results and discussion

Fig. 1 (a) EDS spectrum and (b) XRD pattern of the product obtained at 12 h (V_{EG}:V_E =1:1).

Fig. 1a shows EDS spectrum of the product obtained from the solvothermal reaction time of 12 h when the volume ratio of EG to ethanol is 1:1. The peaks of Bi, O and W elements are found. The atomic ratio of the three elements is 1.96:1:5.91, which is closed to the composition of Bi_2WO_6. Fig. 1b shows the XRD pattern of the as-prepared product. It is clearly seen that eight diffraction peaks at 2θ of 28.3º, 36.0º, 47.2º, 55.9º, 58.6º, 68.6º, 75.9º and 78.3º can be indexed as the monoclinic phase of Bi_2WO_6 with the crystal plane of (103), (202), (220), (303), (107), (400), (109) and (307), which is completely consistent with the standard card (JCPDS NO. 26-1044, a=5.480 Å, b=5.480 Å, c=11.500 Å). The sharp diffraction peaks indicate the high crystallization of the as-prepared Bi_2WO_6. Since no other diffraction peaks and impurity phase, the product is confirmed as a high purity by the solvothermal method.

Fig. 2 (a) FESEM images of Bi_2WO_6 prepared at 12 h (V_{EG}:V_E =1:1), (b) the higher magnification image of Fig. 2a, (c, d) TEM images of the as-prepared Bi_2WO_6.

Figs. 2a, b show the SEM images of the product at the reaction time of 12 h .We can find that Bi_2WO_6 nanoparticles are spherical with flower-like morphology, and the size of microspheres is relatively uniform with an diameter of about 1.5 μm. The broken microsphere indicates the microspheres are hollow. The higher

RSC Advances Accepted Manuscript

This journal is © The Royal Society of Chemistry 201x

magnification image (Fig. 2b) represents that the petal structure of Bi_2WO_6 microsphere is assembled by many nanosheets with an average thickness of about 15 nm, and some pores are shown in the microsphere shell because of the cross-link of nanosheets. The SEM images demonstrate that the structure of Bi_2WO_6 microsphere is porous as well as hollow structure. The hollow structure can also be verified by TEM images in Figs. 2c, d. The contrast of the darker parts and lighter parts indicates the hollow structure. From Fig. 2d, we can know that the darker parts composed of nanosheets are the shell with the average thickness of 250 nm, and the lighter parts in the center of microsphere exhibits the hollow part with the diameter of about 800 nm. The observed results of TEM and SEM images both prove that the as-synthesized products are the porous flower-like hollow microspheres.

Fig. 3 SEM images of the samples at the reaction time of (a) 1 h, (b, c) 4 h, and (d, e) 8 h, (f) XRD patterns of the samples obtained at different reaction stages.

To further investigate the formation mechanism of the highly ordered self-assembled hollow microspheres, we analyze the morphology and phase of the products under different reaction stages.

Fig. 3 shows the SEM images of the samples with the reaction time of 1h, 4 h, and 8 h, respectively. At 1h, the sample exhibits a sphere shape with the diameter of about 150 nm (Fig. 3a). When we extend the reaction time to 4 h, the nanoparticles assembled into the uniform microspheres with rough surface (Figs. 3b, c) and diameter of about 1.2 μm. When the reaction time stretches to 8 h, the outer layer nanoparticles of the microspheres gradually grow into nanosheets, whose thickness is about 10 nm (Figs. 3d, e). The broken microspheres in Fig. 3d indicate the formation of the hollow structure. At the reaction time of 12 h, a highly ordered porous and hollow microspherical structure with a larger diameter (Fig. 2) is obtained by the Ostwald ripening process. The XRD patterns shown in Fig. 3f demonstrate the crystallinity of the samples improves with the increase of the reaction time.

Fig. 4 Schematic illustration of the probable formation mechanism of hierarchical flower-like Bi_2WO_6 hollow spheres.

Fig. 4 shows the possible formation and growth mechanism of the flower-like hollow Bi_2WO_6 microspheres. First, $Bi(NO_3)_3{\cdot}5H_2O$ and $Na_2WO_4{\cdot}2H_2O$ are dissolved in ethylene glycol/ethanol, respectively. When the two solutions are mixed, no precipitation is found (Fig. S1) due to the coordination or hydrogen bond between Bi^{3+} or WO_4^{2-} and -OH of ethylene glycol and ethylene [2, 9]. At the initial stage of solvothermal reaction, Bi^{3+} and WO_4^{2-} are released slowly under the high temperature and high pressure condition to the nucleation and growth of the Bi_2WO_6 nanoparticles via the ionic reaction[10] (Fig. 3a). With the increase of reaction time, these nanoparticles gradually self-assemble to large spheres with rough surface (Fig. 3b, c) to minimize the interfacial energy [11]. Then Ostwald ripening process takes place, the smaller nanoparticles in the center of the large spheres dissolve into the solution. Meanwhile, the oriented growth process is occurred with the formation of nanosheets on the external of the large spheres (Fig. 3d, e) [12, 13]. Finally, the hierarchical flower-like Bi_2WO_6 microspheres with uniform nanosheets are observed in Fig. 2.

Fig. 5 (a) UV-vis diffuse reflectance spectrum and (b) $(\alpha h\nu)^2$ *vs.* $h\nu$ plot of the hollow Bi_2WO_6 microspheres prepared at 12 h (V_{EG}:V_E =1:1).

Fig. 5a shows the UV-visible diffuse reflectance spectrum of the product obtained at 12 h (V_{EG}:V_E =1:1). The absorption edge of the flower-like hollow microspheres is estimated to be about 480 nm, indicating the redshift of peak happened and the absorption range of the flower-like hollow microspheres expanded to the visible region, compared to the commercial Bi_2WO_6 [14].

The optical absorption band edge basic equation of the crystal semiconductor is in accordance with equation (1) [15]:

$$(\alpha h\nu)^2 = A(h\nu - E_g)^n \quad (1)$$

α, ν, E_g and A represent absorption coefficient, optical frequency, width of band gap and a constant, respectively. The n value of Bi_2WO_6 is 1, which determines the transition state of the semiconductor. According to the equation (1), the E_g value of flower-like hollow Bi_2WO_6 microsphere is calculated to be about 2.72 eV from Fig. 5b, which consists with previous work [16].The results suggest that the hollow Bi_2WO_6 may possess good photocatalytic properties when irradiated under visible light.

Fig. 6 N_2 adsorption–desorption isotherm curves and pore size distribution (inset) of the hierarchical flower-like Bi_2WO_6 product.

N_2 adsorption-desorption isotherms and pore size distribution (inset) are employed to evaluate the surface area of the flower-like hollow Bi_2WO_6 microspheres (Fig. 6). The hysteresis of N_2 adsorption-desorption circulation is clearly seen, indicating that the products are porous, which is consistent with the observed morphology of flower-like hollow Bi_2WO_6 microspheres. The specific surface area of the hollow microspheres is 95 $m^2\ g^{-1}$ and the pore volume is 0.97 $cm^3\ g^{-1}$, which are larger than the reported in the previous literatures [17, 18]. The pore size of 36 nm and 92 nm may be caused by the space between the nanosheets. The flower-like hollow microspheres with large specific surface area are benefited to increase the contact efficiency with organic contaminants to improve the photocatalytic activity.

Fig. 7 (a) the temporal evolution of the absorption spectra of the RhB solution (Inset shows the corresponding time-dependent color change of RhB solution, (b) degradation rate of RhB in the presence of hierarchical flower-like hollow Bi_2WO_6 under visible-light irradiation, (c) reused ability of the hollow Bi_2WO_6.

The photocatalytic activity of the synthesized hierarchical flower-like hollow Bi_2WO_6 microspheres in the degradation of RhB is evaluated under visible light at room temperature. The characteristic absorption peak of RhB at 554 nm is used to monitor

RSC Advances Accepted Manuscript

catalytic process. Fig. 7a shows the temporal evolution of the photocatalytic degradation of RhB solution. With the increase of visible light irradiation time, the intensity of the absorption peak of RhB decreases gradually along with the blue shift of the peak. The inset in Fig. 7a shows the dynamic variety of RhB solution color with the degradation time. It is clearly seen that the RhB solution changes gradually from pink to colorless due to the deethylation step by step, generating gradually N, N, N-three ethyl rhodamine, N, N-three ethyl rhodamine, N-ethyl rhodamine and rhodamine. At last, the conjugate structure is destructed into CO_2 and H_2O [19, 20]. Fig. 7b presents the photocatalytic efficiency of the as-synthesized product for the degradation of RhB. It is worth mentioning that the catalytic efficiency of the flower-like hollow Bi_2WO_6 microspheres is 98% for the degradation of RhB under visible-light irradiation within 50 min. It is resulted from the large specific surface area of the flower-like porous shell and the hollow structure of the interior, which could provide many binding sites for the catalysant effectively. Fig. 7c reveals that the catalytic efficiency of the as-synthesized hollow Bi_2WO_6 microspheres still reach more than 92% after five photocatalytic cycles, indicating the stability of the flower-like hollow catalyst.

Fig. 8 SEM images of the Bi_2WO_6 prepared at the reaction time of 12 h with different volume ratios of EG to ethanol: (a) 1:0, (b) 2:1, (c) 0:1, (d) Comparison of the degradation rates of RhB (1.0×10^{-5} mol L^{-1}) in the presence of prepared samples shown in Figs.10 a-c under visible light for 50 min.

Figs. 8a-c shows the SEM images of the samples prepared at the reaction time of 12 h with different volume ratios of EG to ethanol. It is seen that the morphologies of the samples are sensitive to content of the both solvents. When the volume ratio of EG to ethanol is 1:0, the irregular morphologies of Bi_2WO_6 can be observed (Fig. 8a). The hollow spheres with rough surface are detected in Fig. 8b (V_{EG}:V_E=2:1). The hierarchical flower-like Bi_2WO_6 hollow microspheres formed at V_{EG}:V_E = 1:1 are shown in Fig. 2.When the volume ratio of EG to ethanol is 0:1, the blocks are discovered (Fig. 8c). From the above discussion, we conclude that EG and ethanol both play important roles in the formation of products with different morphologies. These samples are further used for the photocatalyze degradation of RhB. It is found that the hierarchical flower-like hollow Bi_2WO_6 prepared at V_{EG}/V_E of 1:1 possesses the best catalytic activity (Fig. 8d).

Fig. 9 Degradation rate of RhB (1.0×10^{-5} mol L^{-1}) in the presence of hierarchical flower-like hollow Bi_2WO_6 at different pH values of solutions: (a) time-dependent, (b) the maximum value under visible-light irradiation for 50 min.

Fig. 9a shows the influence of pH value on the degradation of RhB in the presence of hierarchical flower-like hollow Bi_2WO_6 (V_{EG}:V_E=1:1). As the pH value changes from 4 to 6.5, the photocatalytic degradation rates of RhB increase. When the pH value is more than 8, the degradation rate of RhB gets down. The possible reason is that the Bi_2WO_6 can be easy to hydrolysis into H_2WO_4 and Bi_2O_3 in the acidic solution [21]. In the alkaline solution, amount of OH^- anions lead to the catalyst surface is negatively charged and RhB turned into anion due to the dissociation of –COOH group. The repulsion of Bi_2WO_6 and RhB makes the adsorption between them reduced and impedes the degradation reaction. Another possible reason may be the formation of $Bi_{3.84}W_{0.16}O_{6.24}$ in the alkaline solution, which possesses little photocatalytic activity for degradation of RhB [22]. From Fig. 9b, it is clearly observed that the highest degradation rate of RhB is 98% under visible-light irradiation at the pH value of 6.5. We conclude that the photocatalytic degradation rate of RhB could be controlled by the pH values of solution.

Fig. 10 First-order plots for the degradation of RhB at various initial concentrations in the presence of hierarchical flower-like hollow Bi_2WO_6.

The influence of the initial concentration (C_0) on the degradation rate of RhB in the presence of hierarchical flower-like hollow Bi_2WO_6 is observed in the Fig. 10. The experiment data are fitted by applying a pseudo-first-order model ($\ln C/C_0 = -kt$) to verify the reaction rate constant (k) of degradation of RhB. The k values are 0.0841 min^{-1}, 0.014 min^{-1} and 0.00255 min^{-1} for the initial RhB concentrations of 1.0×10^{-5} mol L^{-1}, 5.0×10^{-5} mol L^{-1} and 1.0×10^{-4} mol L^{-1}, which proving the initial concentration of RhB has a significant effect on the degradation rate of RhB. The degradation rate of RhB is higher when the initial concentration is lower. The above first-order linear relation can be explained by the Langmuir-Hinshelwood model: [21]

$$r = \frac{-dC}{dt} = -\frac{kKC}{1+KC} \qquad (2)$$

K refers to the adsorption equilibrium constant; C is the concentration of RhB solution at the reaction time of t. As for the dilute solution, $KC \leq 1$, because of the weak adsorption of RhB on the surface of the catalyst, the equation (2) can be expressed as follow:

$$r = kKC \qquad (3)$$

Therefore, the degradation reaction of RhB by Bi_2WO_6 is apparent first-order kinetics of the Langmuir-Hinshelwood model due to the chosen of low concentrations of RhB solution in our experiment.

Fig. S3 shows the influence of the catalyst dose on the degradation of RhB (1.0×10^{-5} mol L^{-1}, 50 mL). From Fig. S3b, we can know that k values are increased as the catalyst content varied from 10 mg to 70 mg. According to the equation (3), the degradation time of the same amount of RhB will be reduced, which can be observed in Fig. S3a.The possible reason may be that more photocatalytic active sites can be supplied to absorb more photons, which promote the formation of more electron and hole pairs[23], leading to the increase of degradation rate.

RSC Advances Accepted Manuscript

This journal is © The Royal Society of Chemistry 201x

Figures:

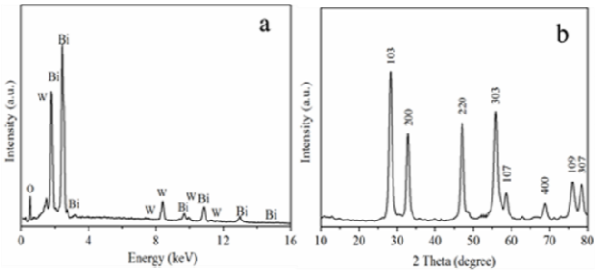

Fig. 1 (a) EDS spectrum and (b) XRD pattern of the product obtained at 12 h (V_{EG}:V_E =1:1).

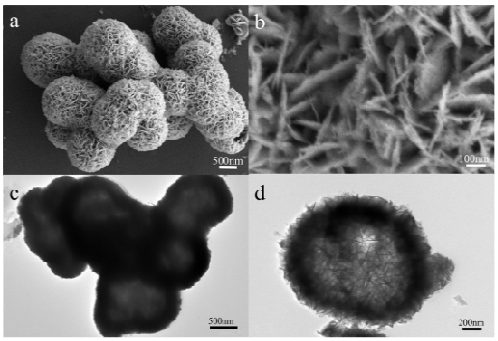

Fig. 2 (a) FESEM images of Bi_2WO_6 prepared at 12 h (V_{EG}:V_E =1:1), (b) the higher magnification image of Fig. 2a, (c, d) TEM images of the as-prepared Bi_2WO_6.

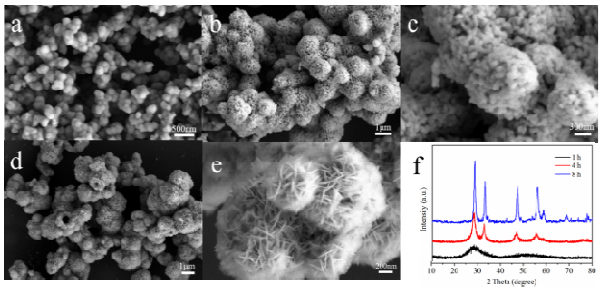

Fig. 3 SEM images of the samples at the reaction time of (a) 1 h, (b, c) 4 h, and (d, e) 8 h, (f) XRD patterns of the samples obtained at different reaction stages.

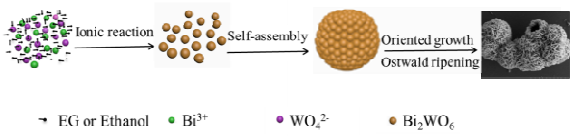

Fig. 4 Schematic illustration of the probable formation mechanism of hierarchical flower-like Bi_2WO_6 hollow spheres.

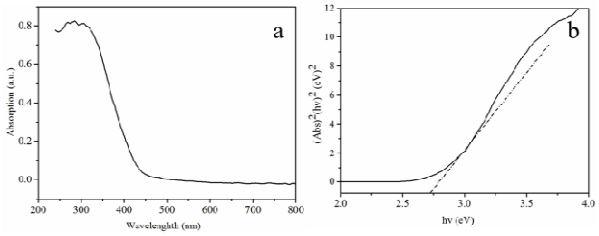

Fig. 5 (a) UV-vis diffuse reflectance spectrum and (b) $(\alpha h\nu)^2$ *vs.* $h\nu$ plot of the hollow Bi_2WO_6 microspheres prepared at 12 h (V_{EG}:V_E =1:1).

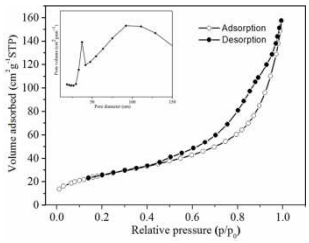

Fig. 6 N_2 adsorption–desorption isotherm curves and pore size distribution (inset) of the hierarchical flower-like Bi_2WO_6 product.

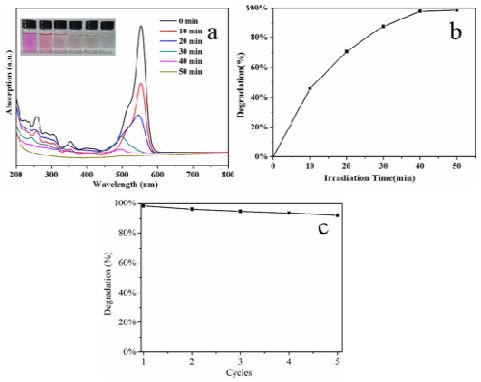

Fig. 7 (a) the temporal evolution of the absorption spectra of the RhB solution (Inset shows the corresponding time-dependent color change of RhB solution, (b) degradation rate of RhB in the presence of hierarchical flower-like hollow Bi_2WO_6 under visible-light irradiation, (c) reused ability of the hollow Bi_2WO_6.

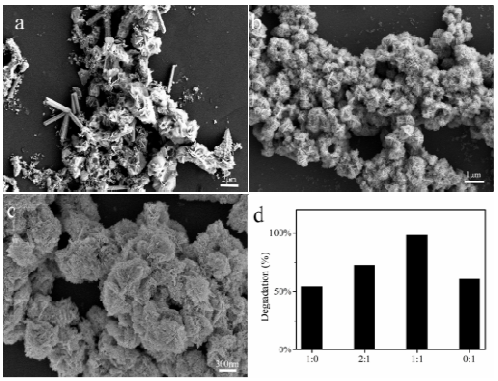

RSC Advances Accepted Manuscript

Fig. 8 SEM images of the Bi_2WO_6 prepared at the reaction time of 12 h with different volume ratios of EG to ethanol: (a) 1:0, (b) 2:1, (c) 0:1, (d) Comparison of the degradation rates of RhB (1.0×10^{-5} mol L^{-1}) in the presence of prepared samples shown in Figs.10 a-c under visible light for 50 min.

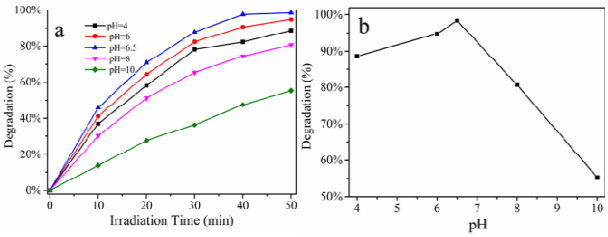

Fig. 9 Degradation rate of RhB (1.0×10^{-5} mol L^{-1}) in the presence of hierarchical flower-like hollow Bi_2WO_6 at different pH values of solutions: (a) time-dependent, (b) the maximum value under visible-light irradiation for 50 min.

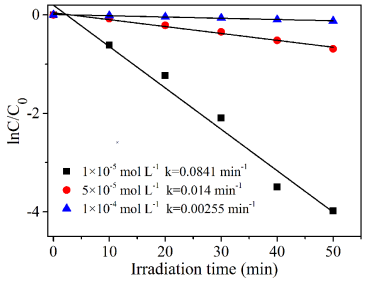

Fig. 10 First-order plots for the degradation of RhB at various initial concentrations in the presence of hierarchical flower-like hollow Bi_2WO_6.

RSC Advances Accepted Manuscript

This journal is © The Royal Society of Chemistry 201x

Conclusions

The hierarchical flower-like Bi_2WO_6 hollow microspheres are synthesized. The hollow Bi_2WO_6 microspheres are assembled by many nanosheets with thickness of about 15 nm. The larger specific surface area of hollow microspheres is favorable for the adsorption of RhB. The hollow Bi_2WO_6 microspheres possess excellent photocatalytic activity as well as the reused ability for the degradation of RhB under visible light. We also find the morphologies of Bi_2WO_6 are affected by the volume ratio of EG to ethanol. The photocatalytic degradation rate of RhB is related to the pH values of solution and morphologies of Bi_2WO_6. This study puts forward a simple and convenient method for fabricating porous and hollow Bi_2WO_6 photocatalyst, providing the possibility of Bi_2WO_6 photocatalyst in treating polluted water.

Acknowledgements

This work is supported by the National Nature Science Foundation of China (No. 91022032, 21173001, and 21371003).

Notes and references

[a] School of Chemistry and Chemical Engineering, Anhui University, Hefei 230601, P. R. China. E-mail: yhshen@ahu.edu.cn; Tel: +860551 63861475

[b] Lab for Clean Energy & Green Catalysis, Anhui University, Hefei 230601, P. R. China

† Electronic Supplementary Information (ESI) available. See DOI: 10.1039/b000000x/

1 H. J. Zhang, G. H. Chen and D. W. Bahnemann, *J. Mater. Chem.*, 2009, 19, 5089-5121.
2 Z. Zhang, W. Wang, D. Jiang and J. Xu, *Appl. Surf. Sci.*, 2014, 292, 948-953.
3 Y. Zhang and Y.J. Xu, *RSC Adv*, 2014, 4, 2904-2910.
4 Y. Y. Li, J. P. Liu, X. T. Huang and G. Y. Li, *Cryst. Growth Des.*, 2007, 7, 1350-1355.
5 F. Amano, K. Nogami, R. Abe and B. Ohtani, *J. Phys. Chem. C*, 2008, 112, 9320-9326.
6 Z. Chen, L. W. Qian, J. Zhu, Y. P. Yuan and X. F. Qian, *Crystengcomm*, 2010, 12, 2100-2106.
7 M. Shang, W. Z. Wang and H. L. Xu, *Cryst. Growth Des.*, 2009, 9, 991-996.
8 C. L. Yan and D. F. Xue, *J. Phys. Chem. B*, 2006, 110, 11076-11080.
9 S.P. Hu, C.Y. Xu and L. Zhen, *Mater. Lett.*, 2013, 95, 117-120.
10 G. Tian, Y. Chen, W. Zhou, K. Pan, Y. Dong, C. Tian and H. Fu, *J. Mater. Chem.*, 2011, 21, 887-892.
11 C. C. Yec and H. C. Zeng, *J. Mater. Chem. A*, 2014, 2, 4843-4851.
12 X. Wang, L. Chang, J. Wang, N. Song, H. Liu and X. Wan, *Appl. Surf. Sci.*, 2013, 270, 685-689.
13 C. Xu, X. Wei, Y. Guo, H. Wu, Z. Ren, G. Xu, G. Shen and G. Han, *Mater. Res. Bull.*, 2009, 44, 1635-1641.
14 Y. Yan, Y. Wu, Y. Yan, W. Guan and W. Shi, *J. Phys. Chem. C*, 2013, 117, 20017-20028.
15 J. Zhang, Y. Wang, S. Li, X. Wang, F. Huang, A. Xie and Y. Shen, *CrystEngComm*, 2011, 13, 5744-5750.
16 B. Zhao, M. Wang, L. Lin, Q. Zeng and D. He, *Cera. Int.*, 2014, 40, 5831-5835.
17 Y. Liu, H. Tang, H. Lv, Z. Li, Z. Ding and S. Li, *Cera. Int.*, 2014, 40, 6203-6209.
18 G. Zhu, J. Liang, M. Hojamberdiev, S. Aldabe Bilmes, X. Wei, P. Liu and J. Zhou, *Mater. Lett.*, 2014, 122, 216-219.
19 Y. Li, J. Liu and X. Huang, *Nanoscale Res. Lett.*, 2008, 3, 365-371.
20 W. Xiong, Q. Zhao, X. Li and D. Zhang, *Catal. Commun.*, 2011, 16, 229-233.
21 H. b. Fu, C. S. Pan, W. Q. Yao and Y. F. Zhu, *J. Phys. Chem. B* 2005, 109, 22432-22439.
22 C. Xu, X. Wei, Z. Ren, Y. Wang, G. Xu, G. Shen and G. Han, *Mater. Lett.*, 2009, 63, 2194-2197.
23 H. b. Fu, W. Q. Yao, L. W. Zhang and Y. F. Zhu, *Mater. Res. Bull.*, 2008, 43, 2617-2625.

RSC Advances Accepted Manuscript